Hardness, Microstructure and Surface Characterization of Laser Gas Nitrided Commercially Pure Titanium Using High Power CO_2 Laser

J. Senthil Selvan, K. Subramanian, A.K. Nath, A.K. Gogia, A.K. Balamurugan, and S. Rajagopal

(Submitted 28 January 1998; in revised form 27 May 1998)

Surface nitriding of commercially pure (CP) titanium was carried out using high power CO_2 laser at pure nitrogen and dilute nitrogen (N_2 + Ar) environment. The hardness, microstructure, and melt pool configuration of the laser melted titanium in helium and argon atmosphere was compared with laser melting at pure and dilute nitrogen environment. The hardness of the nitrided layer was of the order of 1000 to 1600 HV. The hardness of the laser melted titanium in the argon and helium atmosphere was 500 to 1000 HV. Using x-ray analysis the formation of TiN and Ti_2N phase was identified in the laser nitrided titanium. The presence of nitrogen in the nitrided zone was confirmed using secondary ion mass spectroscopy (SIMS) analysis. The microstructures revealed densely populated dendrites in the sample nitrided at 100% N_2 environment and thinly populated dendrites in dilute environment. The crack intensity was large in the nitrided sample at pure nitrogen, and few cracks were observed in the 50% N_2 + 50% Ar environment.

Keywords dendritic microstructure, laser gas alloying, laser nitriding, laser surface modification, titanium nitride

1. Introduction

The technique of developing TiN coating on the metal surface is a widely accepted process in industries. The TiN coating has unique properties such as low density (5.43 g cm^{-3}), good electrical resistance (ρ = 21.7 $\mu\Omega$ cm at 20 °C), thermal, mechanical, chemical properties, high hardness, good friction coefficient, abrasive resistance, low Young's modulus, and gold colorization (Ref 1). Due to these excellent properties, TiN can be used as wear resistance coating in aircraft landing gear (Ref 2) and as an anticorrosive coating in aeroengine turbine blades in aircraft industries (Ref 3). TiN coating can also improve the corrosion and erosion resistance of steel material (Ref 4 to 8) and tribological properties of titanium and titanium alloys.

Titanium and titanium alloys are extensively used in aerospace industries due to their outstanding properties, such as low density, good strength to weight ratio, fracture toughness, corrosion resistance, and bio compatibility. In many applications because of poor wear performance, the use of these alloys in severe frictional condition is restricted (Ref 9). To increase wear resistance, the surface property has to be improved. Surface coatings such as anodizing, electroless nickel plating, hard chrome plating, and plasma spraying are useful in improving the tribological property of titanium alloys (Ref 10). In addition to these coatings, the creation of TiN on the surface of titanium can improve the wear resistance. Various processes are currently available to coat TiN in the surface of titanium, which include, for instance, plasma vapor deposition (Ref 11), chemical vapor deposition (Ref 12), reactive direct current (dc) magnetron sputtering (Ref 13), ion implantation (Ref 14), plasma nitriding (Ref 9, 15, 16, 17), and plasma spraying technique (Ref 18). Except plasma spraying process, all of the previously mentioned techniques produce a very thin TiN layer of thickness 2 to 50 μm. In addition to this fact, these techniques require high vacuum for the deposition of TiN layer. This limitation can be overcome by the newly developed technique, the laser surface modification process, which can give a hard layer of thickness 0.5 to 1.0 mm, and vacuum is not required for producing the TiN layer. It can be produced by laser melting the titanium alloys in gaseous or liquid nitrogen atmosphere (Ref 19, 20). The effect of laser nitriding under pure nitrogen atmosphere was discussed by Kloosterman and De Hossen (Ref 21) and Bell et al (Ref 22).

In this paper, the authors have discussed the effect of nitriding in pure and dilute nitrogen (N_2 + Ar) environment, and the result was compared with laser melted titanium in pure helium and argon environment. The nitrided layer was characterized using optical microscopy, x-ray diffraction (XRD), hardness, and secondary ion mass spectrometry (SIMS) analysis.

J. Senthil Selvan and **K. Subramanian,** Department of Physics, Anna University, Chennai 600 025, India; **A.K. Nath,** Centre for Advanced Technology, Indore, Madya Pradesh, India; **A.K. Gogia,** DMRL, Kanchanbagh, Hyderabad, India; and **A.K. Balamurugan** and **S. Rajagopal,** Materials Science Division, Indira Gandhi Centre for Atomic Research, Kalpakkam-603 102, Tamil Nadu, India.

2. Experimental Detail

2.1 Laser Processing

Laser melting experiments were carried out using 5 kW CO_2 laser (indigenously designed at the Center for Advanced Technology, Indore, India). A constant laser beam power of 1.5 kW with 1 mm beam diameter was made to irradiate the workpiece surface at a traverse speed of 0.5 m min^{-1}. The specimen was laser processed in pure argon, helium, nitrogen, and dilute nitrogen environment. The dilution of nitrogen with argon gas was

arranged by controlling the partial pressure of the respective gases. The raw beam of diameter 25 mm was finely focused into a circular beamof diameter 1 mm on the metal surface by using a 2.5 in. zinc-selenide lens. The shielding gas was fed through coaxial nozzle. In addition to this, there was also a side flow through a nozzle fitted at an angle of 45° to the workpiece surface.

2.2 Material

Commercial pure titanium of size 100 by 50 by 4 mm^3 was used for laser processing. Before laser processing, the surface was roughened with 220 and 320 grit paper and then degreased in a solution containing HF, HNO_3, and H_2O.

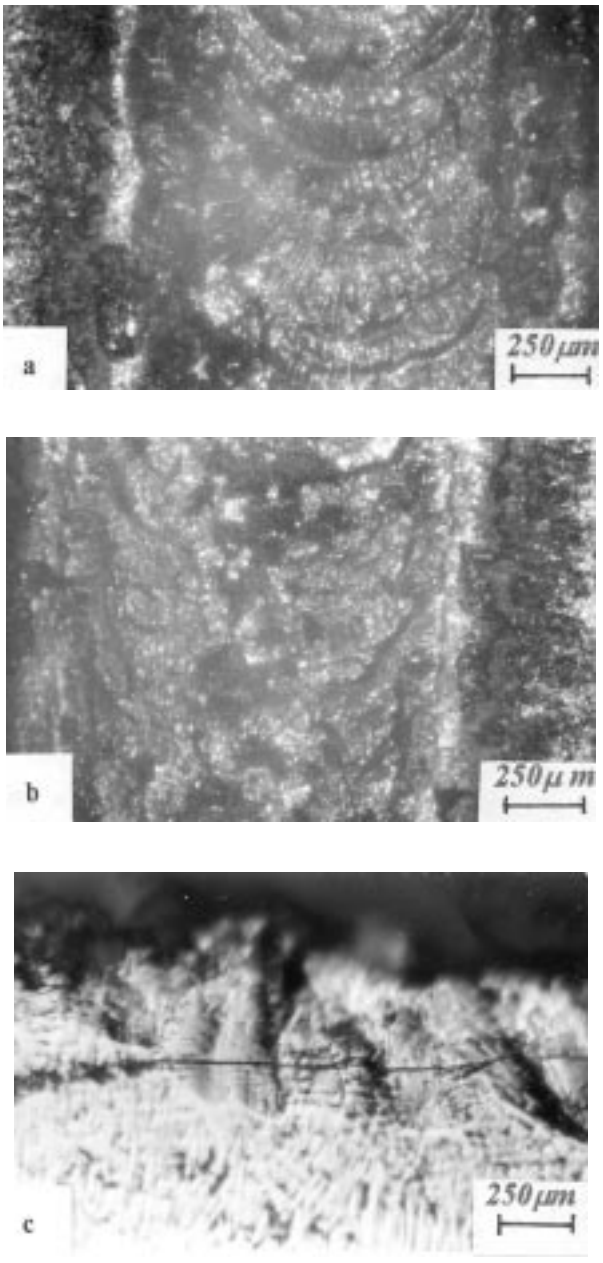

Fig. 1 (a) Surface ripple waves. (b) Surface crack across the laser nitrided track. (c) Appearance of parallel crack inside the nitrided surface in 100% N_2 environment

2.3 Characterization

The laser melted sample sectioned to its melt direction was polished using standard metallographic procedure. To reveal the microstructure the polished surface was etched in Keller's reagent (5 mL HF + 10 mL HNO_3 + 85 mL H_2O). The surface appearance, cracking, melt pool configuration, and microstructure were examined using an Olympus optical microscope. With the Schimadzu microhardness tester, the hardness across the depth of the laser melted zone was determined. The phases present in the nitrided specimen were identified by XRD analysis. The extent of nitrogen diffusion within the laser nitrided zone was investigated using SIMS (CAMECA ims 4f, CAMECA Instruments, Inc., Trumbull, CT) line profile analysis and mass spectrum.

3. Results and Discussion

3.1 Ripple Formation and Cracks in the Nitrided Layer

The appearance of white color was noticed in the laser nitrided surface layer. No golden color was observed. The white surface observed in the nitrided layer was due to the impurity oxygen present in the shielding gas. The surface rippling in the nitrided layer was observed under optical microscopic examination. The rippling waves were formed in a semicircular pattern (Fig. 1a). The surface rippling was attributed to the surface tension gradient and temperature gradient in the laser nitrided layer. Because of the Gaussian profile of laser beam, the temperature formed at the center of the beam surface was higher than at its periphery. This produces surface temperature gradient on the alloyed track. At the edge of the track, the surface tension force was larger, and near the center of the beam surface, it decreased to a lower value. The largest surface tension force at the edge of the track pulls the liquid from the central area in a rapid speed. Hence the flow of molten liquid was toward the edge. As the beam moved away, the rapid solidification resulted, and so the frozen area appeared in the form of rippling waves. From Fig. 1(a), it was also identified that the flow pattern was toward its alloying direction.

Besides the surface ripples, microcracks appeared across the nitrided track (Fig. 1b). The visual examination did not show any cracking on the surface and was viewed by optical microscope under 50×. The crack intensity in pure nitrogen and dilute nitrogen atmosphere was very high. This was also observed in an argon and helium atmosphere. Because the processing was carried out in lower scan speed, the cracking was observed in all the cases (Table 1). The cracking can be eliminated if the processing is carried out at larger scan speed and also by preheating the substrate. Except in a pure nitrogen environment, the cracking was observed only at the surface. But, the crack propagated inside the alloyed layer was observed in a pure nitrogen atmosphere (Fig. 1c). This behavior was imputed to the brittle behavior of intense TiN dendrites formed near the surface region.

Table 1 The surface crack detail, alloying depth, and width of laser melted commercially pure titanium at pure helium, argon, N_2, and dilute nitrogen environment

Environment	Crack intensity	Surface conditions	Alloying depth, mm	Alloying width, mm
Helium	0.02	Smooth and bright white surface	0.28	1.0
Argon	0.3	Smooth and bright white surface	0.3	1.2
Nitrogen, 100%	1.0	Rough and bright white surface	1.5	1.4
Nitrogen, 87.5% + Argon, 12.5%	1.0	Rough and bright white surface	0.35	1.2
Nitrogen, 75% + Argon, 25%	1.0	Rough and bright white surface	0.33	1.1
Nitrogen, 50% + Argon, 50%	0.6	Smooth and bright white surface	0.35	1.1
Nitrogen, 25% + Argon, 75%	0.08	Smooth and bright white surface	0.45	1.3

Laser power, 1.5 kW; beam diameter, 1 mm; scan speed, 0.5 m/min; power density, 1.9×10^5 W/cm^2; laser energy density, 22.8 kJ/cm^2

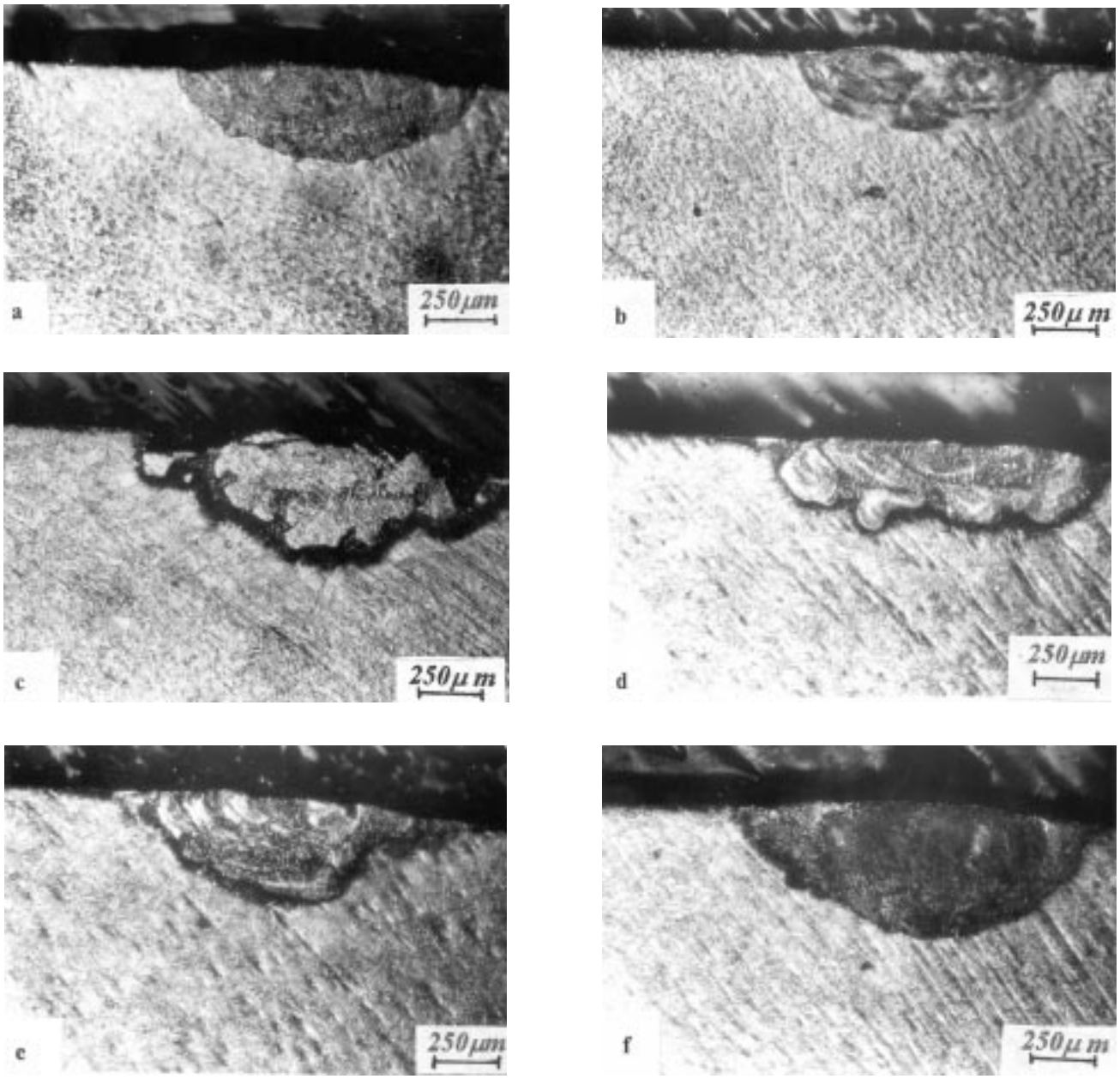

Fig. 2 Transverse cross section profile of laser melted titanium in (a) 100% Ar, (b) 100% He, (c) 100% N_2, (d) 75% N_2 + 25% Ar, (e) 50% N_2 + 50% Ar, and (f) 25% N_2 + 75% Ar environment. (Scale: 1 cm = 250 μm)

3.2 Alloying Depth and Width

The melt depth and width of the laser processed titanium largely depend on the cover gas environment. Table 1 shows that the alloying depth and width at pure and dilute nitrogen environment was larger than that obtained in an argon or helium atmosphere. The shallow depth and width obtained in laser melted titanium at a pure helium and argon environment was due to its nonreactive nature with titanium. The higher heat transfer ability and the reactive nature of nitrogen gas with titanium increase the alloying depth and width (Ref 23, 24). This can be further explained in the following way. The diatomic nitrogen gas rapidly dissociates and ionizes at high temperature due to the plasma formation at the workpiece surface during the

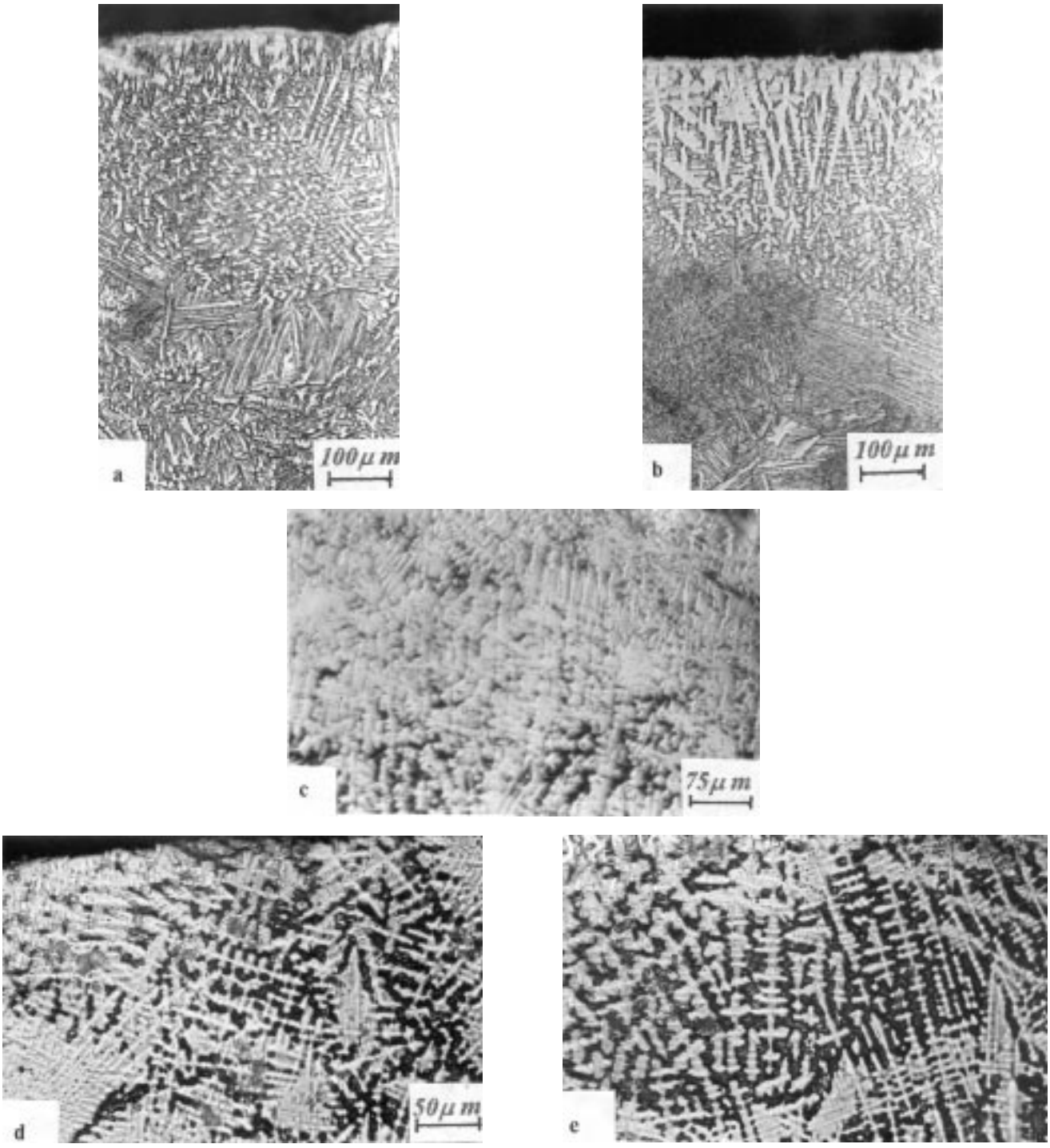

Fig. 3 The microstructures observed in the laser melted CP titanium at (a) 100% Ar, (b) 100% He, (c) 100% N_2, (d) 75% N_2 + 25% Ar, and (e) 50% N_2 + 50% Ar atmosphere. (Largely populated dendrites are seen in 100% N_2.)

laser interaction. It recombines at the work piece surface and increases the heat transfer ability (Ref 25), which favors the large alloying depth. The monoatomic helium and argon gas will not dissociate chemically, so the heat transfer efficiency becomes less, which decreases the depth of melt track. The deeper alloying depth at pure nitrogen atmosphere and shallow depth in argon, helium, and dilute nitrogen ($Ar + N_2$) atmosphere may be attributed to the downward flow of the liquid metal and the radially outward flow of the melt pool respectively (Ref 26).

3.3 Melt Pool Configuration

The shape of the laser melted area depends upon the shielding gas. The transverse cross section of Fig. 2(a) to (f) shows the profile of the laser melted titanium in pure argon, helium, N_2, and dilute nitrogen environment. From this profile, it was observed that the melt configuration was regular and uniform in argon, helium, and 25% N_2 + 75% Ar environment. Whereas, at pure and partially diluted nitrogen atmosphere, the shape of the melt pool was irregular and poor. The interface was severely affected at pure nitrogen atmosphere. The distortions near the interface and irregular shape of the melt pool can be attributed to several factors. The flatness and the irregularities of the melt pool were not due to the laser processing parameters but depend on the following properties:

- The chemical reaction of nitrogen with molten titanium. In this case, the TiN layer formed instantaneously on the surface during nitridation, restrict or slowed the nitrogen diffusion inside the melt pool. This increase of TiN at the surface layer enhances its viscosity, which can also influence the final surface morphology.
- Thermal gradient during the solidification process (Rayleigh convection). Secondly, due to the instabilities in the convective flow, the thermal gradient on the melt pool imposed the internal stress, which may also result in the irregular shape nitrided layer.
- The surface tension inhomogeneity (Marangoni convection). Finally, the surface tension gradient originated either from the thermal gradient at the surface or local perturbations in the concentration of the alloyed layer may have caused the protrusions near the transition region. The irregularities in the surface tension directly depend upon the Marangoni number (Ref 27). If the Marangoni number is positive, the melt pool is uniform and will flatten the isotherm. If the sign is negative, the convection effect is opposite and the isotherm curvature is reinforced.

3.4 Optical Microscopic Examination

The microstructures observed in the laser melted zone at the argon, helium, 100% N_2, 75% N_2 + 25% Ar, and 50% N_2 + 50% Ar atmospheres were shown in Fig. 3(a) to (e), respectively. The martensite and dendrite microstructure were observed in the argon and helium atmosphere. The dendrite structure observed near the surface at the helium atmosphere was attributed to high cooling rate. In this condition, the possibility of forming a hard ceramic layer will not occur.

When nitriding at pure nitrogen atmosphere (Fig. 3c), the formation of a thick dendrite layer was observed. In this case, the chemical reaction between the nitrogen molecule and molten titanium was very high due to the higher nitrogen concentration. So the dendrite population level was large near the surface. The larger diffusion of nitrogen caused the fine dendrites. The less populated dendrites were observed near the transition region. The TiN formed near the surface minimize the diffusion of nitrogen inside the molten layer and decreased the reaction of nitrogen with titanium. Near the transition region, few nitrogen atoms were participated in the chemical reaction with molten titanium. Hence, the dendrite population near the transition region was decreased.

Further, the decrease in dendrite population was noticed when nitrogen was diluted with argon. This effect was clearly noticed from microstructures obtained in 100% N_2, 75% N_2 + 25% Ar, and 50% N_2 + 50% Ar atmospheres (Fig. 3c, d, e). In dilute atmosphere, the presence of monoatomic argon gas minimizes the nitrogen diffusion and its reaction with titanium melt, so the thickness of dendrite population was decreased to a large extent.

In the case of nitriding in a pure nitrogen environment, the plasma generated during laser interaction with the workpiece rapidly dissociated the nitrogen molecule and increased the diffusion of nitrogen in the molten titanium.

3.5 Microhardness Determination

The hardness measurements were made on samples laser melted in argon, helium, pure nitrogen, and dilute nitrogen environments using a Vickers microhardness tester at 200 g load. Figure 4 (a) to (c) shows the hardness profile taken at these conditions. The hardness of laser melted CP titanium at argon and helium environment was in the range of 500 to 700 HV and 600 to 900 HV, respectively. The high hardness of 900 HV at the laser melted surface in helium atmosphere can be attributed to the hard dendrite microstructure (Fig. 3b).

At 100% N_2 condition, a high hardness of 1400 to 1500 HV and 700 to 1200 HV was observed near the surface and the bottom layer of the laser nitrided zone, respectively. The very low hardness of 500 HV obtained at the surface at 100% N_2 condition was due to the brittle behavior of thickly populated TiN dendrites.

In the dilute nitrogen environment (Fig. 4b), the large variation in hardness was observed, and it can be attributed to the inhomogeneous concentration of TiN dendrites. The hardness of 800 to 1600 HV was observed when a larger amount of nitrogen was diluted with argon (82.5% N_2 + 27.5% Ar, 75% N_2 + 25% Ar, and 50% N_2 + 50% Ar), but it decreased to 500 to 950 HV at 25% N_2 + 75% Ar environment.

The high hardness of 1400 to 1600 HV and 800 to 1400 HV observed in the laser nitrided zone was attributed to the presence of TiN and Ti_2N ceramic phases, respectively. The dendrite precipitates in the α-titanium may also have caused the formation of high hardness. The low hardness, 500 to 600 HV, obtained in the heat affected zone was due to the presence of needle-shaped martensitic structure. The hardness of CP titanium was approximately 165 HV. The high hardened nitrided zone with hard TiN ceramic phase can improve the wear resistance and load carrying capability.

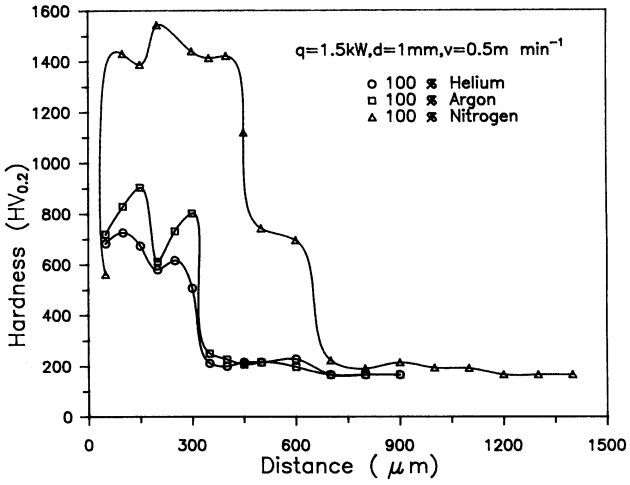

(a)

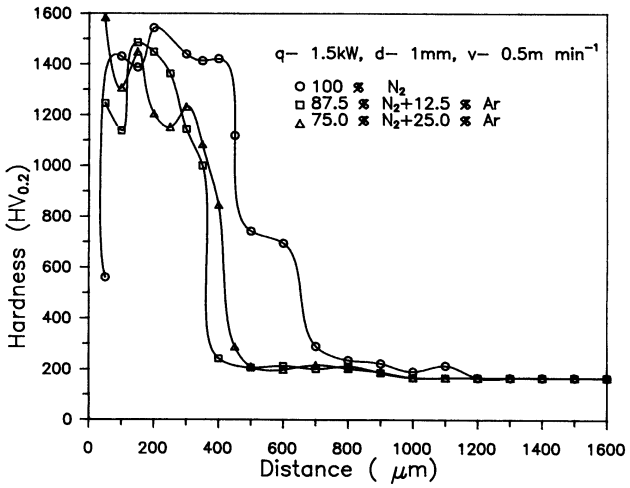

(b)

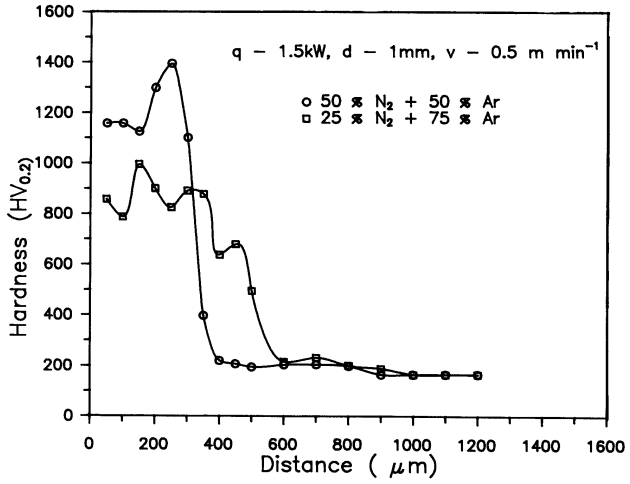

(c)

Fig. 4 (a) Comparison of microhardness profile of laser melted CP titanium in pure 100% Ar, 100% He, and 100% N_2 environment. (b) Microhardness profile of laser melted CP titanium in 100% N_2, 82.5% N_2 + 27.5 Ar, and 75% N_2 + 25% Ar environment. (c) Microhardness profile of laser melted CP titanium in 50% N_2 + 50% Ar, and 25% N_2 + 75% Ar environment

3.6 X-Ray Analysis

Using XRD study, the TiN and Ti_2N phases present in the laser nitrided zone (100% N_2) was identified (Fig. 5). The large intensity peak in Fig. 5 can be related to the high content TiN formed at the surface. The high hardness obtained in the nitrided area was imputed to the formation of TiN dendrites, which was confirmed from XRD and microhardness study.

3.7 Secondary Ion Mass Spectroscopy Analysis

The diffusion of nitrogen in the nitrided area cannot be precisely determined using energy dispersive analysis because of its low yield. In addition, the energy peaks on nitrogen and titanium (L peak) do overlap due to its bad resolving power. Hence the authors have carried out SIMS analysis to identify the nitrogen diffusion in the laser nitrided zone. The analysis was made with cesium (Cs) primary ion beam operated at 10 keV. The secondary ions emitted from the laser nitrided zone analyzed by a double focusing (energy sector followed by a magnetic mass analyzer) spectrometer and collected by the electron multiplier was used to determine the nitrogen content. Figure 6(a) and (b), respectively, show SIMS line profile analysis carried out through the depth and parallel to the width (50 μm below the surface) of the laser nitrided area. The line profile shows the presence of nitrogen in the laser-alloyed zone, whereas the unmelted titanium did not show any nitrogen content. Thus it can be confirmed that, during laser alloying nitrogen gas environment, the dissociated nitrogen molecule in the laser plasma was diffused into the molten pool and formed a chemical reaction with titanium melt. The small variation of nitrogen peak in the laser alloyed zone can be attributed to the compositional variation of nitrogen in the dendrite and inter-dendrite region. The sharp rise and fall of nitrogen intensity in the line profile was due to the dense dendrites and inter-dendrite region, respectively. Also, the SIMS mass spectrum was taken by sputtering the nitrided zone in a sampling area of 50 μm with Cs^+ primary ion beam. From the SIMS mass spectrum, it is possible to identify the compound formed within the alloyed layer. The SIMS mass spectrum (Fig. 7) shows intense Ti^+ and Cs Ti^+ peak. The

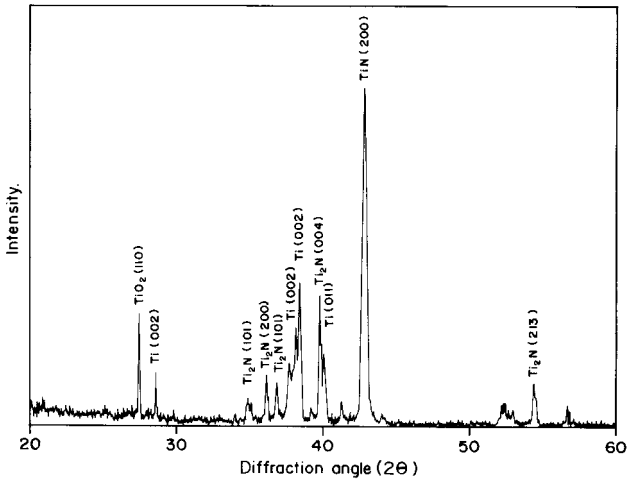

Fig. 5 X-ray diffraction (XRD) profile of laser nitrided CP titanium at 100% N_2 atmosphere.

peak at mass number 14 related to the nitrogen, which was diffused during the nitriding process. The hard ceramic compound phase TiN, Ti_2N, and Cs TiN complex was identified at atomic mass numbers 62, 110, and 195, respectively. The singly and doubly ionized titanium (Ti I and Ti II) was related to the titanium peaks at mass number 48 and 24, respectively.

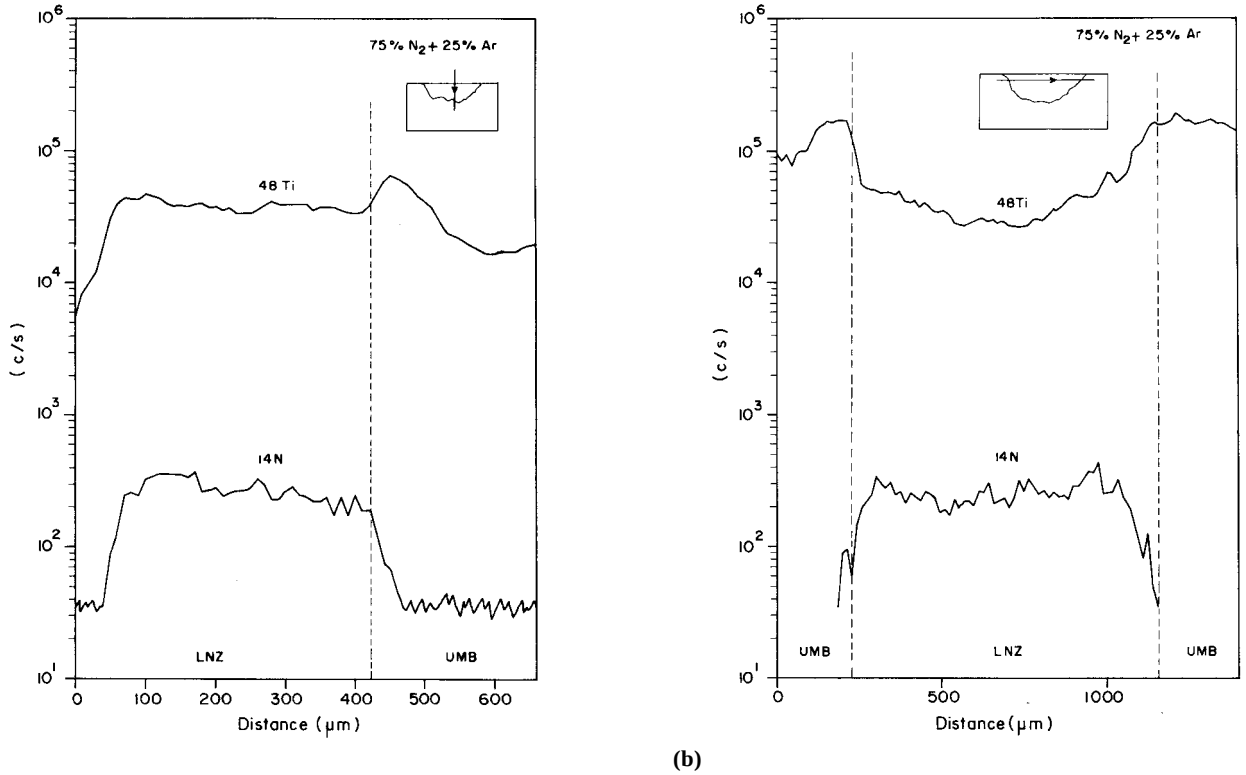

Fig. 6 Secondary ion mass spectroscopy (SIMS) line profile recorded at laser nitrided CP titanium (a) across the depth of the nitrided zone, (b) parallel to the width (50 μm below the surface) of the laser nitrided area (unmelted base, or UMB; laser nitrided zone, or LNZ)

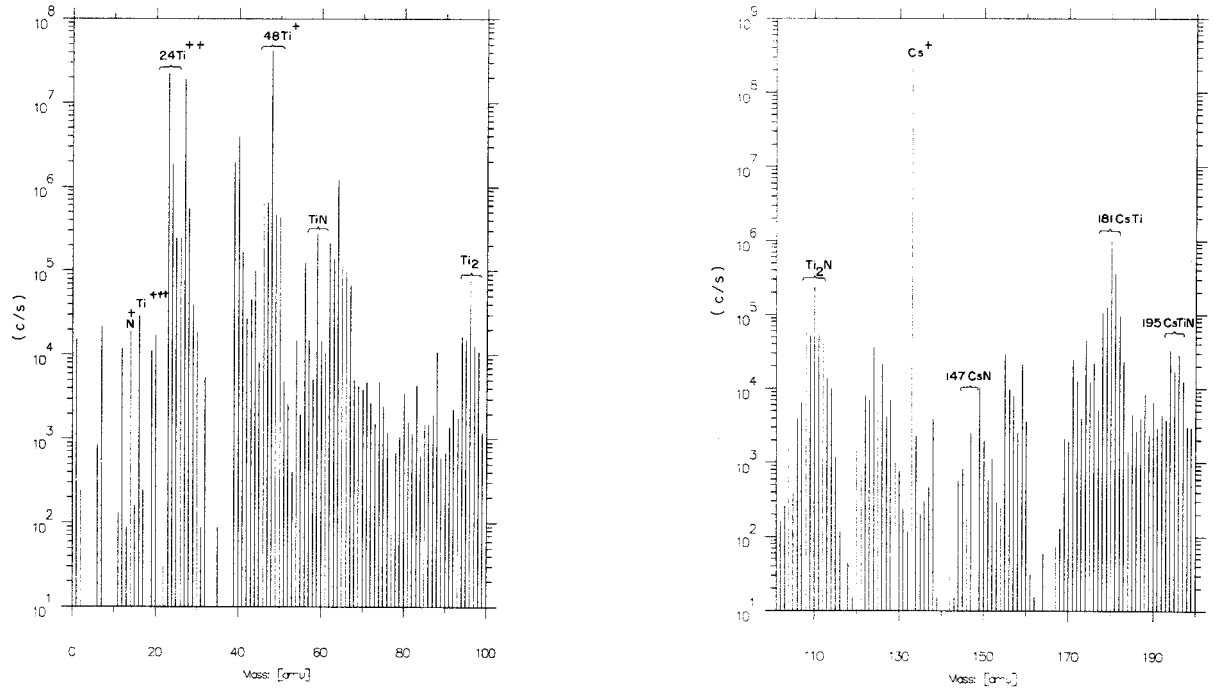

Fig. 7 Secondary ion mass spectroscopy (SIMS) mass spectrum recorded inside the nitrided layer shows 48 Ti^+, 24 Ti^{++}, 133 Cs^+, 181 Cs Ti^+, 14 N^+, 62 TiN^+, 110 Ti_2N^+, and 195 Cs TiN^+

3.8 Surface Temperature Estimation

The temperature evolved at the workpiece surface during laser irradiation can be roughly estimated using the simple relation (Ref 28):

$$T_o = (P\eta/r\lambda)\,[0.147 - 0.054 \ln (vr/4a)] \quad \text{(Eq 1)}$$

where P is laser power, η is absorptivity, λ is coefficient of thermal conductivity, a is thermal diffusivity, v is travel speed, and r is beam radius. The temperature estimation during the laser nitriding process can be useful to predict the diffusion of nitrogen and the resulting TiN formation.

Ursu et al. (Ref 19, 20) have studied the absorption behavior of titanium and zirconium in technical nitrogen using microsecond pulsed (transversely excited atmosphere pressure, TEA) CO_2 laser irradiation. The absorptivity of TiN at 10.6 μm radiation was in the range 9 to 14%. Whereas, the absorptivity of titanium in nitrogen environment at one atmospheric pressure was approximately 15% during the interaction of first few laser pulses. Therefore in this study, the authors have estimated the surface temperature by assuming the absorptivity of titanium metal as 15%.

The estimated surface temperature in this laser processing condition (laser power 1.5 kW, beam radius 0.5 mm, and speed 0.5 m min^{-1}) was approximately 5000 °C. So, at this high temperature of 5000 °C, plasma generated at the workpiece surface during laser irradiation dissociates the diatomic nitrogen, and instantaneously the dissociated nitrogen atoms diffused into the molten titanium. All this process occurred in a solidification time of 0.12 s (solidification time = beam diameter/travel speed). Within this short duration the diffusion nitrogen chemically reacted with molten titanium; on rapid solidification, TiN can be formed within the melting range of approximately 3000 °C.

4. Conclusions

The laser melting of commercially pure titanium was carried out in pure helium, argon, nitrogen, and dilute nitrogen environments using the high power CO_2 laser. The results were summarized as follows:

- The laser nitrided titanium surface shows cracks. Cracks appeared at the laser nitrided surface, but the intensity of cracks was minimum when nitriding at 50% N_2 + 50% Ar environment. The cracks at a depth of 50 μm were observed parallel to the width of the nitride track in the 100% nitrogen atmosphere. Crack formation can be prevented by the preheating technique or by nitriding at higher traverse speed.
- The laser melting in argon and helium environment produced a hardness of 600 to 950 HV. A very high hardness of 1200 to 1600 HV was obtained in pure nitrogen and dilute (82.5% N_2 + 27.5% Ar, 75% N_2 + 25% Ar, and 50% N_2 + 50% Ar) nitrogen atmospheres. It is significant to note that the nitrided layer produced a hardness of 6.0 to 9.6 times more than the base metal. The high hardness obtained by the laser nitriding technique can improve the wear resistance and load carrying capability.
- The microstructures in the laser nitrided zone were comprised of dendrites. The degree of dendrite formation depended upon the partial pressure and concentration of the nitrogen gas. The dendrite population in pure nitrogen environment was higher than in the dilute environment.
- The laser nitrided zone consists of a hard ceramic TiN phase.
- The diffusion of nitrogen in the laser nitrided layer was verified using SIMS line profile analysis. The TiN and Ti_2N phases present in the nitrided area were identified using SIMS mass spectrum.

References

1. A. Gicquels, N. Laidani, P. Saillard, and J. Amoaroux, Plasma and Nitrides: Application to the Nitriding of Titanium, *Pure Appl. Chem.*, Vol 62 (No. 9), 1990, p 1743-1750
2. B.L. Mordike, Applications of Laser Surface Melting, *ECLAT '96—Proc. 6th European Conf. on Laser Treatment of Materials* (Stuttgart, Germany), F. Dausinger, H.W. Bergmann, and J. Sigel, Ed., 1996, p 253-262
3. Y. Massiani, A. Medjahad, P. Gravier, and J.P. Crousier, Effects of Titanium Underlayer on the Corrosion Behavior of Physically Vapor Deposited Titanium Nitride Films, *Thin Solid Films*, Vol 217, 1992, p 31-37
4. M.B. Karamis, Friction and Wear Behavior of Plasma Nitrided Layer on 3%Cr-Mo Steel, *Thin Solid Films*, Vol 202, 1991, p 49-60
5. Tribological Behavior of Plasma Nitrided 722M24 Material Under Dry Sliding Conditions, *Wear*, Vol 147, 1991, p 385-399
6. J. Glusek, J. Kadrkowiak, J. Masalki, and W. Popytak, Ti and TiN Coatings on 316L Surgical Steel, *Surface Engineering Practice, Process, Fundamentals and Applications in Corrosion and Wear*, N.N. Strafford, P.K. Datta, and J.S. Gray, Ed., Ellis Horwood Limited, U.K., 1990, p 233-241
7. L. Chen, Electrochemical Studies of TiN Coated SS Steel, *Plat. Surf. Finish.*, Vol 79 (No. 1), 1992, p 58-63
8. P.J. Burnett and D.S. Rickerby, The Corrosion Behavior of TiN Coatings on Steels, *J. Mater. Sci.*, Vol 23 (No. 7), 1988, p 2429-2443
9. M. Muraleedharan and E.J. Meletis, Surface Modification of Pure Titanium and Ti-6Al-4V by Intensified Plasma Ion Nitriding, *Thin Solid Films*, Vol 221, 1992, p 104-113
10. A. Bloyce, H. Dong, and B. Hanson, Comparative Evaluation of Treatments for Wear Protection of Ti-6Al-4V, *Titanium '95: Science and Technology*, The Institute of Materials, London, 1996, p 1975-1982
11. K.-H. Habig, Friction and Wear of Sliding Couples Coated with TiC, TiN or TiB_2, *Surf. Coat. Technol.*, Vol 42, 1990, p 133-147
12. M.R. Hilton, M. Salmeron, and G.A. Somorjai, The Effect of Argon during the Plasma Assisted Chemical Vapor Deposition of TiN, *Thin Solid Films*, Vol 167, 1988, p L31-L34
13. M.K. Wahlstrom, E. Johansson, E. Veszelei, P. Bennich, M. Olsson, and S. Hogmork, Improved Langmuir Probe Surface Coatings for the Cassini Satellite, *Thin Solid Films*, Vol 220, 1992, p 315-320
14. S. Saritas, R.P.M. Procter, and W.A. Grant, The Use of Ion Implantation to Modify the Tribological Properties of Ti-6Al-4V, *Mater. Sci. Eng.*, Vol 90, 1987, p 297-306
15. B. Tesi, A. Molinari, G. Straffelini, T. Bacci, and G. Pradelli, Ion Nitriding Temperature Influence on Tribological Characteristics of Ti-6Al-4V Alloy, *Titanium '95: Science and Technology*, The Institute of Materials, London, 1996, p 1983-1990

16. B.S. Yilbas, A. Coban, J. Nickel, M. Sunar, M. Sami, and B.J. Abdul Aleem, Investigation into Nitrided Spur Gears, *J. Mater. Eng. Perform.*, Vol 5, 1996, p 728-733
17. A. Kobayashi, Surface Nitridation of Titanium Metal by Means of Gas Tunnel Type Plasma Jet, *J. Mater. Eng. Perform.*, Vol 5, 1996, p 373-380
18. M. Fukumoto, S. Itoh, and S. Itoh, Fabrication of Functionally Graded TiN Coating by Reactive Plasma Spraying, *Surf. Eng.*, Vol 13 (No. 4), 1997, p 315-319
19. I. Ursu, I.N. Mihailescu, L.C. Nistor, A. Popa, M. Popescu, V.S. Teodorescu, L. Nanu, A.M. Prokhorov, V.I. Konov, V.N. Tokarev, and S.A. Uglov, Titanium and Zirconium Nitridation under the Action of Microsecond Pulsed TEA CO_2 Laser Irradiation in Technical Nitrogen, *J. Phys. D, Appl. Phys.*, Vol 18, 1985, p 1693-1700
20. I. Ursu, I.N. Mihailescu, L. Nanu, L.C. Nistor, M. Popescu, V.S. Teodorescu, A.M. Prokhorov, V.I. Konov, S.A. Uglov, and V.G. Raichenkov, Nitridation of Ti and Zr by Multipulse TEA CO_2 Laser Irradiation in Liquid Nitrogen, *J. Phys. D, Appl. Phys.*, Vol 19, 1986, p 1183-1188
21. A.B. Kloosterman and J.T.M. De Hossen, Microstructural Characterization of Laser Nitrided Titanium, *Scr. Metall. Mater.*, Vol 33 (No. 4), 1995, p 567-573
22. T. Bell, M.H. Sohi, J.R. Betz, and A. Bloyce, Energy Beams in Second Generation Surface Engineering of Aluminium and Titanium Alloys, *Scand. J. Metall.*, Vol 19, 1990, p 218-226
23. W. Lucas, Shielding Gas for Arc Welding, Part I, *Weld. Met. Fabr.*, Vol 60 (No. 6), 1992, p 218-225
24. F. Bultmann, Influence of Different Shielding Gases and Welding Parameters on the Weld Quality in Tungsten Inert Gas Welding with Dual Gas Shield, *Schweissen Schneiden*, Vol 47, 1995, p E150-E153
25. M.H. Glowacki, The Effects of the Use of Different Shielding Gas Mixtures in Laser Welding of Metals, *J. Phys. D, Appl. Phys.*, Vol 28, 1995, p 2051-2059
26. S. Kou and Y.H. Wang, Weld Pool Convection and its Effect, *Weld. J.*, Vol 65, 1986, p 63s-70s
27. P.J. Desre and J.C. Coub, Surface Tension Temperature Coefficient of Liquid Alloys and Definition of a "Zero Marangoni Number Alloy" for Crystallization Experiments in Microgravity Environment, *Acta Astronautica*, Vol 8 (No. 5-6), 1981, p 407-415
28. S. Eskin, J. Zahavi, and A. Berner, CO_2 Laser Nitriding as a Result of Ti Coating Modification in a Nitrogen Atmosphere, Part I—Feature of Nitriding Process, *Lasers Eng.*, Vol 4, 1995, p 85-96